

Observation of topological crystalline insulator surface states on (111)-oriented $\text{Pb}_{1-x}\text{Sn}_x\text{Se}$ filmsC. M. Polley,^{1,*} P. Dziawa,² A. Reszka,² A. Szczerbakow,² R. Minikayev,² J. Z. Domagala,² S. Safaei,² P. Kacman,² R. Buczko,² J. Adell,¹ M. H. Berntsen,^{3,†} B. M. Wojek,³ O. Tjernberg,³ B. J. Kowalski,² T. Story,² and T. Balasubramanian¹¹*MAX IV Laboratory, Lund University, 221 00 Lund, Sweden*²*Institute of Physics, Polish Academy of Sciences, 02-668 Warsaw, Poland*³*KTH Royal Institute of Technology, ICT Materials Physics, Electrum 229, 164 40 Kista, Sweden*

(Received 12 December 2013; revised manuscript received 11 February 2014; published 28 February 2014)

We present angle-resolved photoemission spectroscopy measurements of the surface states on *in-situ* grown (111) oriented films of $\text{Pb}_{1-x}\text{Sn}_x\text{Se}$, a three-dimensional topological crystalline insulator. We observe surface states with Dirac-like dispersion at $\bar{\Gamma}$ and \bar{M} in the surface Brillouin zone, supporting recent theoretical predictions for this family of materials. We study the parallel dispersion isotropy and Dirac-point binding energy of the surface states, and perform tight-binding calculations to support our findings. The relative simplicity of the growth technique is encouraging, and suggests a clear path for future investigations into the role of strain, vicinality, and alternative surface orientations in (Pb,Sn)Se solid solutions.

DOI: [10.1103/PhysRevB.89.075317](https://doi.org/10.1103/PhysRevB.89.075317)

PACS number(s): 73.20.At, 71.20.-b, 79.60.-i, 81.15.-z

I. INTRODUCTION

Following the first experimental report in 2008 of photoemission from the unusual surface states associated with a three-dimensional topological insulator (TI) [1], these materials have attracted a rapidly developing research interest [2]. More than simply fertile new ground for research into quantum phenomena, topological insulators have much to offer in spintronic and quantum computation applications due to their spin-polarized, topologically protected interface states.

For the initially studied class of Z_2 invariant topological insulators, the gapless nature of these surface states is topologically protected by time reversal symmetry. A well studied example is the (111) facet of Bi_2Se_3 , in which a solitary Dirac cone resides at $\bar{\Gamma}$ in the surface Brillouin zone (SBZ) [Fig. 1(a)]. An odd number of Dirac cones within the SBZ (in this case one) is one of the defining characteristics of the Z_2 topological insulators.

Recently it was realized that the concept of topological protection can be extended to other symmetries beyond that of time reversal. For the case of point-group symmetries, this gives rise to the new class of “topological crystalline insulators” (TCI) [3,4], though as highlighted in a recent theoretical study mirror symmetry and time reversal symmetry protection need not be mutually exclusive [5]. To date mirror-symmetry protected TCI surface states have been experimentally observed on the (100) faces of $\text{Pb}_{1-x}\text{Sn}_x\text{Se}$ [6–9], $\text{Pb}_{1-x}\text{Sn}_x\text{Te}$ [10,11], and SnTe [12,13]. For all three TCI materials studied to date, angle-resolved photoemission (ARPES) studies of the (100) facet show an even number of band inversions, originating from projections of the L points in the bulk Brillouin zone. Spin-polarized Dirac-like surface states are observed close to each \bar{X} point in the SBZ [Fig. 1(b)], and are protected by the mirror symmetry about the {011} crystal planes. The projection of two inequivalent bulk L points

to the same \bar{X} point in the SBZ gives rise to a complex Fermi surface which exhibits a Lifshitz transition as a function of the chemical potential [4].

The fundamental role of crystalline symmetry in this new family of topological materials makes the study of different surface orientations attractive. Differing degrees of mirror symmetry are retained for different orientations, with important consequences for the low-energy electronic structure. This concept has been discussed at length in recent theoretical studies [14,15] encompassing (100), (110), and (111) surfaces of the (Pb,Sn)Te system. In contrast to the previously studied (100) facets, on the (111) facet each bulk L point is projected to a unique, time-reversal invariant momentum in the SBZ [$\bar{\Gamma}$ and each \bar{M} , Fig. 1(c)]. The proposed existence of a symmetrical $\bar{\Gamma}$ surface state with high Fermi velocity and simple spin texture is appealing from the perspective of potential device applications. There is hence strong motivation for an experimental photoemission spectroscopy study of (111) oriented materials, to advance both fundamental and applied aspects of TCI research.

However a practical difficulty encountered when studying non-(100) surface orientations within the (Pb,Sn)Te or (Pb,Sn)Se material classes is the lack of natural cleavage planes. In all previous experimental studies, pristine (100) surfaces could be obtained by *in-situ* cleaving of an *ex-situ* prepared bulk crystal. This method is constrained to the set of natural cleavage planes in the bulk crystal, and hence precludes studying arbitrary surface orientations. Here we report the *in-situ* growth and angle-resolved photoemission spectroscopy characterization of (111) oriented $\text{Pb}_{1-x}\text{Sn}_x\text{Se}$ films. The demonstrated ease of growing such films should widen the scope of future studies in this family of TCI materials.

II. EPITAXIAL LAYER GROWTH

Films were grown on BaF_2 substrates, which were cleaved in air to expose a fresh (111) facet and then attached to silicon base plates to enable direct current heating. After entry into ultra high vacuum (UHV), substrates were outgassed at 600 °C for one hour, then reduced to a temperature of 330 °C for the film growth. Films of $\text{Pb}_{1-x}\text{Sn}_x\text{Se}$ were

*craig.polley@maxlab.lu.se

†Present address: Deutsches Elektronen-Synchrotron (DESY), Photon Science, Coherent X-ray Scattering, Notkestrasse 85, 22607 Hamburg, Germany.

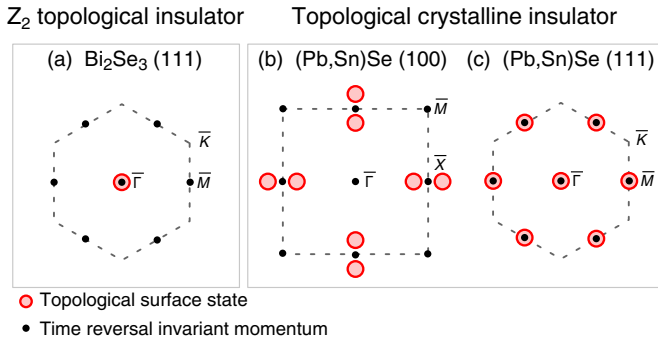


FIG. 1. (Color online) A schematic comparison of Z_2 TIs with TCIs. The Z_2 TI Bi_2Se_3 (a) exhibits a single Dirac cone in the (111) SBZ; in general an odd number of Dirac cones is a defining property of Z_2 TIs. TCI materials such as $(\text{Pb,Sn})\text{Se}$ have previously been studied with a (100) surface orientation (b), and exhibit four Dirac cones close to each \bar{X} . Here we study (111) oriented $(\text{Pb,Sn})\text{Se}$ (c), predicted to exhibit Dirac-like states at each time reversal invariant momentum (four of which are unique).

deposited onto the BaF_2 using an open hot wall epitaxy method [16]. Single-source evaporators were used, consisting of filament heated quartz crucibles loaded with *ex-situ* recrystallized $\text{Pb}_{1-x}\text{Sn}_x\text{Se}$. Both $x = 0.24$ and $x = 0.27$ sources were used in the present study. After establishing a crucible temperature of $\approx 330^\circ\text{C}$ (maintaining vacuum pressure below 1×10^{-8} mbar), a substrate was positioned over the crucible mouth for 100 minutes. Subsequent analysis with cross-sectional electron microscopy indicates that this corresponds to a film thickness of (900 ± 50) nm.

Structural characterization of the grown layers is summarized in Fig. 2. Crucially for the present study, low energy electron diffraction [Fig. 2(a)] consistently exhibits a (111) pattern, indicating that the grown films have assumed the orientation of the BaF_2 substrate. A representative sample grown from the $x = 0.27$ source was selected for more comprehensive characterization, including reciprocal space mapping using $\text{Cu-K}\alpha_1$ x-rays and a high resolution diffractometer, as shown in Fig. 2(b). Symmetrical reciprocal space maps of the 111 reflection for both the substrate (lower feature) and layer

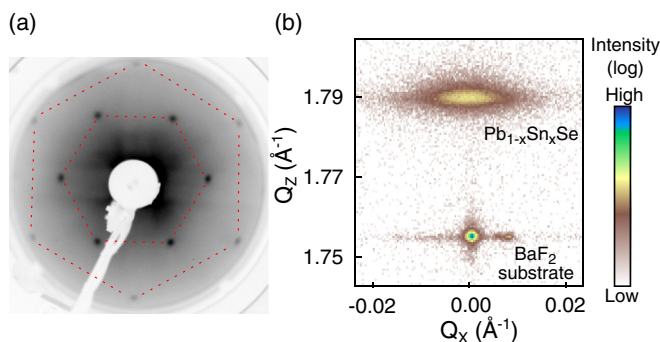


FIG. 2. (Color online) (a) Low energy (111 eV) electron diffraction of the grown film, demonstrating two orders of a 111 reflection pattern. (b) Reciprocal lattice map using symmetrical $\text{Cu-K}\alpha_1$ x-rays, 111 Bragg reflection. The upper feature corresponds to the grown layer and the lower to the BaF_2 substrate.

(upper feature) are shown. The grown layer exhibits a higher mosaicity than the substrate, with an angular spread reaching a full width at half maximum of approximately 0.5° . The shape of the upper pattern demonstrates a well defined lattice constant (6.08 \AA) which can be mapped to a molar fraction of $x = (0.37 \pm 0.01)$ [17]. Additional reciprocal space maps (not shown here) of the 115 asymmetric reflection indicate that the grown layer is not strained at room temperature.

Quantitative composition analysis by energy dispersive x-ray spectroscopy (EDX) indicates a Sn content of $x = (0.36 \pm 0.01)$, laterally uniform throughout the film and in good agreement with the value calculated from reciprocal space mapping. This is higher than the source material ($x = 0.27$) but is still suitable for the observation of a band-inverted condition [6]. We note that in this temperature range evaporation occurs molecularly as PbSe and SnSe [18]. Consequently, while the higher vapor pressure of SnSe compared to PbSe may result in differences between the chemical composition of the source and the grown layer, reasonable preservation of the source composition is possible with a simple, single source evaporation method.

Taken together, the characterization studies demonstrate that epitaxial, compositionally uniform (111) oriented $\text{Pb}_{1-x}\text{Sn}_x\text{Se}$ films were produced by this growth method, with a Sn content appropriate for the existence of topological surface states. This is essential for the validation of ARPES measurements, which we now discuss.

III. PHOTOEMISSION MEASUREMENTS

The film growth was performed on the I4 beam line at the MAX-III synchrotron facility [19], allowing for extensive ARPES characterization without leaving UHV. All spectra were acquired with linearly *p*-polarized photons at a sample temperature of ≈ 100 K. The photoelectron analyzer was configured for an energy resolution of 25 meV and angular resolution of $\approx 0.1^\circ$. Fermi level positions were referenced to a tantalum foil in electrical contact with the samples.

The key result of this study is the observation of surface states with Dirac-like dispersion, occurring at the $\bar{\Gamma}$ and the \bar{M} positions in the SBZ. Before studying these states in detail, we first provide confirmation that they are indeed surface states. In Fig. 3 we show the results of photon energy dependent ARPES measurements. For the $\bar{\Gamma}$ state seen at normal emission, such a measurement probes the Γ - L high symmetry direction in the bulk Brillouin zone. Normal emission energy distribution curves [Fig. 3(a)] show a broad dispersive peak (attributed to the bulk L_6 band) together with a sharper, dispersionless peak at a binding energy of 70 meV. The lack of perpendicular dispersion is more clearly apparent in the parallel momentum resolved spectra shown in Fig. 3(b), and combined with its position within a bulk band gap serves to confirm that this second peak originates from a surface state.

While the position of the surface state is unchanged when varying the photon energy, the intensity of the state is strongly modulated. The highest intensity is observed at approximately $h\nu = 18.5$ eV; the bulk-state dispersion shown in Fig. 3(a) suggests that this energy probes the L_6 valence band maximum. In Fig. 3(c) we illustrate this modulation more clearly by plotting the intensity ratio of the surface

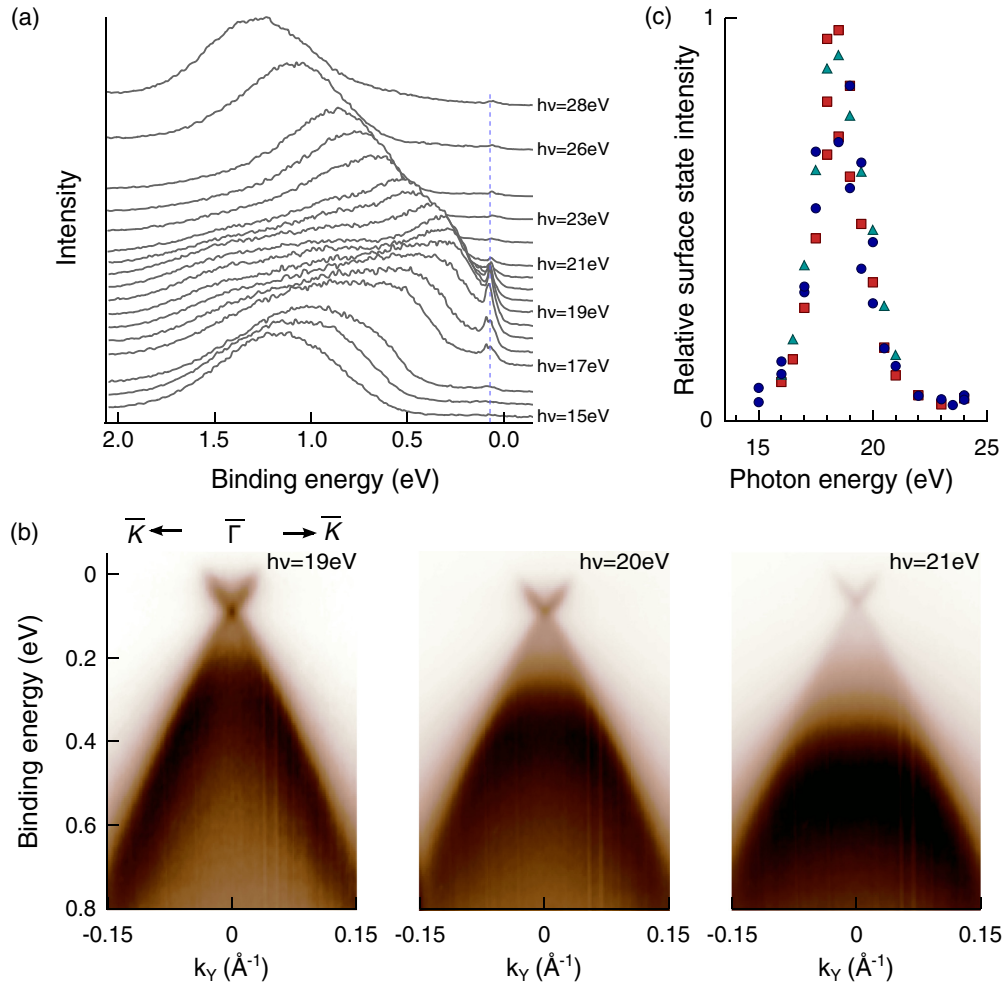


FIG. 3. (Color online) Overview of the role of photon energy in photoemission spectra acquired at $\bar{\Gamma}$. Normal emission energy distribution curves are plotted in (a), normalized to the same maximum intensity and offset according to the excitation photon energy. A sharp state close to the Fermi level is seen which exhibits no perpendicular momentum dispersion. This is most clearly seen in parallel momentum resolved spectra (b), and signifies that this is a surface state. The intensity of the surface state relative to the nearby bulk band is strongly dependent on the choice of photon energy, shown in (c) for multiple sample preparations (indicated by different markers).

state to the bulk L_6 band. Similar intensity modulations were observed at approximately 68 eV and 148 eV. Periodic modulation of photoemission intensity with photon energy is a common observation for surface states [22–24], with an accepted explanation in terms of a resonant enhancement of the coupling between initial and final states in the photoexcitation process [25]. The enhancement is strongest for perpendicular momenta which minimize the energy separation between the surface state and bulk band it derives from. In the present case, this implies resonance peaks at photon energies which probe the bulk valence band maxima at L points. Periodic enhancement was also observed for the \bar{M} surface state, although here the off-normal geometry complicates the interpretation of intensity variations. While usually weaker in intensity than the $\bar{\Gamma}$ state, the states at \bar{M} became visible at a photon energy of ≈ 24 eV. Even choosing this energy, the intensity was approximately 10 times less than that of the $\bar{\Gamma}$ state. A detailed study of the intensity variations is ongoing.

Figure 4 shows energy-momentum ARPES spectra acquired through $\bar{\Gamma}$ ($k_x = 0 \text{ \AA}^{-1}$) and \bar{M} ($k_x = 0.84 \text{ \AA}^{-1}$). Both

spectra were measured on a sample grown from $\text{Pb}_{0.76}\text{Sn}_{0.24}\text{Se}$ source material, from which the highest quality data was obtained. Although the composition was not characterized for this sample, there was no observable difference in the band structure compared to samples grown from the $\text{Pb}_{0.73}\text{Sn}_{0.27}\text{Se}$ source, suggesting a similar composition.

Figure 4(a) compares the dispersion along perpendicular cuts for the $\bar{\Gamma}$ and \bar{M} surface states. While the \bar{M} state possesses asymmetric intensity, within the experimental resolution both states appear to be circularly symmetrical, particularly at the Fermi level [Fig. 4(b)]. In SnTe and $\text{Pb}_{0.4}\text{Sn}_{0.6}\text{Te}$ [14,15] much stronger dispersion anisotropy is expected for the \bar{M} surface state, with faster dispersion along the $\bar{M}-\bar{K}$ cut compared to the $\bar{M}-\bar{\Gamma}$ cut. The origin of this anisotropy can be understood by noting that the surface states here derive from the anisotropic bulk bands at the L points, which are projected onto the (111) surface Brillouin zone [Fig. 4(c)]. The $\bar{M}-\bar{\Gamma}$ direction cuts through the long axis of the bulk constant energy ellipsoids at L , giving rise to a slower dispersion. In Figs. 4(a) and 4(b), such anisotropy is very slight if present at all. This observation is

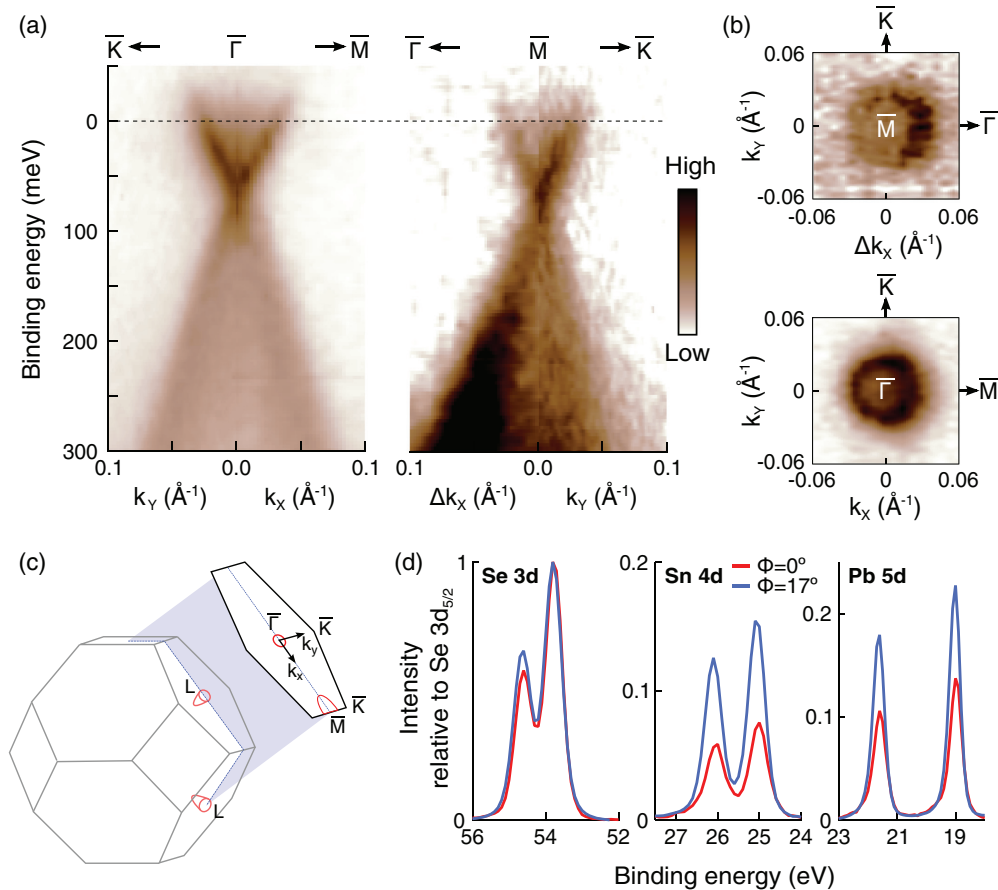


FIG. 4. (Color online) Photoemission spectra of the surface states on a (111) oriented $\text{Pb}_{1-x}\text{Sn}_x\text{Se}$ film. (a) Energy-momentum spectra along high-symmetry lines at $\bar{\Gamma}$ ($k_x = 0 \text{ \AA}^{-1}$) and \bar{M} ($k_x = 0.84 \text{ \AA}^{-1}$) show the presence of Dirac-like surface states at both locations. The location of these states within the SBZ follow from the projection of the bulk L points. These projections exist on $\{110\}$ mirror planes, schematically shown for bulk Fermi ellipsoids in (c). Fermi-surface maps (b) show that the $\bar{\Gamma}$ state is circularly symmetrical, and that the anisotropy of the \bar{M} state is very slight at the Fermi level. Comparing normal ($\phi = 0^\circ$) with off-normal ($\phi = 17^\circ$) emission core-level spectra (d) indicates a cation-rich surface, consistent with the Dirac point residing close to the bulk valence band. Spectra were acquired using photon energies of 17.5 eV ($\bar{\Gamma}$), 24 eV (\bar{M}) and 130 eV (core levels).

consistent with the reduced eccentricity of the Fermi ellipsoids in PbSe compared to PbTe [20] and is reproduced by the tight binding calculations we will discuss shortly.

The Dirac points in Fig. 4(a) are positioned at a binding energy of ≈ 70 meV, a value found to be similar across all sample preparations. As anticipated for a (111) surface with cationic termination, the Dirac points sit close to the bulk valence band maxima. Angle dependent core level spectroscopy [Fig. 4(d)] provide supporting evidence that the surface is indeed rich in Sn and Pb cations. Within the experimental resolution, no relative binding energy difference can be observed between the $\bar{\Gamma}$ and \bar{M} Dirac points. This is again quite different from calculations for telluride materials, for which the \bar{M} Dirac point is predicted to be 30 meV ($\text{Pb}_{0.4}\text{Sn}_{0.6}\text{Te}$) [14] to 45 meV (SnTe) [15] higher in binding energy than the $\bar{\Gamma}$ Dirac point. We highlight that differences in Dirac point binding energies are highly relevant for the interpretation of low-energy transport measurements [21].

Finally we note that while the weak surface states at \bar{M} could potentially be explained as surface-umklapp replicas of the $\bar{\Gamma}$ state, such an interpretation would require both a solitary

metallic surface state at $\bar{\Gamma}$ and a (2×2) surface reconstruction. The former is at odds with numerous theoretical studies of this material system, while the latter is not supported by LEED images acquired over a wide energy range.

IV. BAND STRUCTURE CALCULATIONS

To further investigate our experimental characterization of the (111) surface states (in particular the surface state dispersion anisotropy and Dirac point energy positions), we have performed tight-binding (TB) calculations for a (111) oriented cation terminated slab consisting of 451 layers (≈ 80 nm thick). We have used the virtual crystal approximation for the solid solution of PbSe and SnSe, both in rock-salt structure, using temperature-dependent tight binding parameters described previously [7]. In this approach it has been assumed that the evolution of the TB parameters are dominated by the change in the lattice constant a_0 . Thus the parametrization has been rescaled according to the Harrison rules [26], while it has been assumed that the change in a_0 for any (Pb,Sn)Se solid solution follows the same temperature dependence as that

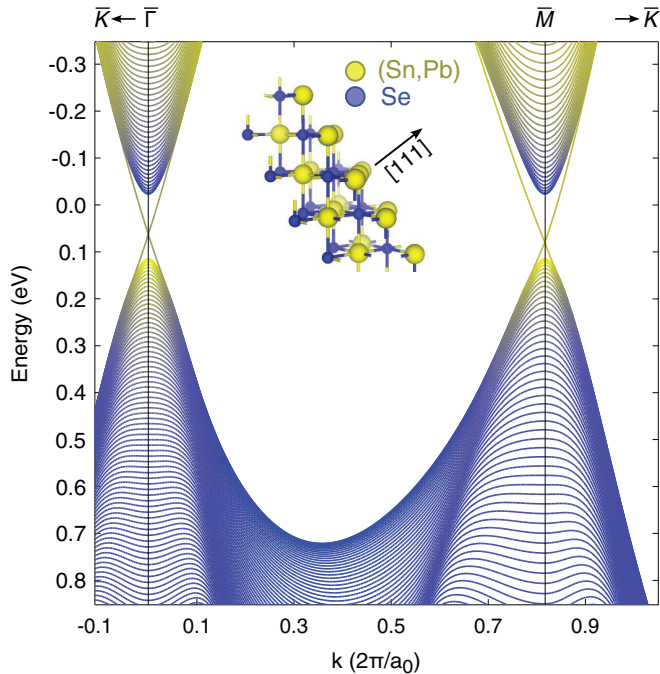


FIG. 5. (Color online) The calculated band structure of a (111) oriented and cation terminated $\text{Pb}_{0.64}\text{Sn}_{0.36}\text{Se}$ slab along high-symmetry directions, using lattice parameters corresponding to a temperature of 100 K ($a_0 = 6.06$ Å). The line color denotes the relative contribution of cation (yellow) or anion (blue) p -type orbitals to the wave function. The inset lattice model indicates why it is necessary to specify the termination type for the (111) orientation, and illustrates the cationic termination used in the calculations.

of PbSe [27]. The room temperature a_0 for $\text{Pb}_{0.64}\text{Sn}_{0.36}\text{Se}$ is taken from x-ray diffraction experiments [17]. We note that while TB parameters for PbSe can be taken from the literature, the parameters for rock-salt SnSe are not available as SnSe crystallizes in an orthorhombic structure. Hence the parametrization of rock-salt SnSe is based solely on the results of density functional theory calculations. Despite this, the qualitative aspects of the band structure are well captured [7].

As shown in Fig. 5, the band calculations for $\text{Pb}_{0.64}\text{Sn}_{0.36}\text{Se}$ for the anticipated lattice parameters at $T = 100$ K indicate an inverted band structure with Dirac-like surface states at $\bar{\Gamma}$ and

\bar{M} . The offset of the energy scale is arbitrary, and has hence been chosen to facilitate comparison with the experimental data. Within the experimental resolution, both the dispersion anisotropy and the difference between the $\bar{\Gamma}$ and \bar{M} Dirac-point binding energies are in agreement with the experimental ARPES spectra in Fig. 4. Thus the observed differences between the surface states observed on $\text{Pb}_{0.64}\text{Sn}_{0.36}\text{Se}$ and those predicted for $\text{Pb}_{0.64}\text{Sn}_{0.36}\text{Te}$ or SnTe can be ascribed solely to the differences between telluride- and selenide-based materials.

V. CONCLUSIONS

By growing (111) oriented $\text{Pb}_{1-x}\text{Sn}_x\text{Se}$ films *in-situ* at a synchrotron ARPES facility, we have been able to spectroscopically measure the topological crystalline insulator states unique to this surface orientation. In contrast to the (100) facet, the Dirac-like surface states are well separated and noninteracting, located at the time reversal invariant momenta $\bar{\Gamma}$ and \bar{M} in the surface Brillouin zone. Our observations are captured by a tight binding model, and provide experimental support for the existing body of theoretical work studying the role of surface orientations in TCI materials. Finally, our demonstration of successfully growing and measuring (Pb,Sn)Se films constitutes an important step towards future studies, enabling investigations into novel transport devices [28], the role of strain [29] (through lattice-mismatch from different substrates), and additional surface orientations [for example the (110) surface].

Note added in proof. Recently, we became aware of a similar study on (111) oriented SnTe [30].

ACKNOWLEDGMENTS

This work was made possible through support from the Knut and Alice Wallenberg Foundation, the Swedish Research Council, the European Commission Network SemiSpinNet (PITN-GA-2008-215368), the European Regional Development Fund through the Innovative Economy Grant (No. POIG.01.01.02-00-108/09), and the Polish National Science Centre (NCN) Grant No. 2011/03/B/ST3/02659. P.D. and B.J.K. acknowledge support from the Baltic Science Link project coordinated by the Swedish Research Council, VR. We thank Jacek Osiecki for creating data analysis software used in this study.

[1] D. Hsieh, D. Qian, L. Wray, Y. Xia, Y. S. Hor, R. J. Cava, and M. Z. Hasan, *Nature (London)* **452**, 970 (2008).
 [2] Y. Ando, *J. Phys. Soc. Jpn.* **82**, 102001 (2013).
 [3] L. Fu, *Phys. Rev. Lett.* **106**, 106802 (2011).
 [4] T. H. Hsieh, H. Lin, J. Liu, W. Duan, A. Bansil, and L. Fu, *Nat. Commun.* **3**, 982 (2012).
 [5] T. Rauch, M. Fliieger, J. Henk, I. Mertig, and A. Ernst, *Phys. Rev. Lett.* **112**, 016802 (2014).
 [6] P. Dziawa, B. J. Kowalski, K. Dybko, R. Buczko, A. Szczerbakow, M. Szot, E. Łusakowska, T. Balasubramanian, B. M. Wojek, M. H. Berntsen, O. Tjernberg, and T. Story, *Nat. Mater.* **11**, 1023 (2012).

[7] B. M. Wojek, R. Buczko, S. Safaei, P. Dziawa, B. J. Kowalski, M. H. Berntsen, T. Balasubramanian, M. Leandersson, A. Szczerbakow, P. Kacman, T. Story, and O. Tjernberg, *Phys. Rev. B* **87**, 115106 (2013).
 [8] A. Gyenis, I. K. Drozdov, S. Nadj-Perge, O. B. Jeong, J. Seo, I. Pletikoscic, T. Valla, G. D. Gu, and A. Yazdani, *Phys. Rev. B* **88**, 125414 (2013).
 [9] Y. Okada, M. Serbyn, H. Lin, D. Walkup, W. Zhou, C. Dhital, M. Neupane, S. Xu, Y. J. Wang, R. Sankar, F. Chou, A. Bansil, M. Z. Hasan, S. D. Wilson, L. Fu, and V. Madhavan, *Science* **341**, 1496 (2013).

- [10] S.-Y. Xu, C. Liu, N. Alidoust, M. Neupane, D. Qian, I. Belopolski, J. D. Denlinger, Y. J. Wang, H. Lin, L. A. Wray, G. Landolt, B. Slomski, J. H. Dil, A. Marcinkova, E. Morosan, Q. Gibson, R. Sankar, F. C. Chou, R. J. Cava, A. Bansil, and M. Z. Hasan, *Nat. Commun.* **3**, 1192 (2012).
- [11] Y. Tanaka, T. Sato, K. Nakayama, S. Souma, T. Takahashi, Z. Ren, M. Novak, K. Segawa, and Y. Ando, *Phys. Rev. B* **87**, 155105 (2013).
- [12] Y. Tanaka, Z. Ren, T. Sato, K. Nakayama, S. Souma, T. Takahashi, K. Segawa, and Y. Ando, *Nat. Phys.* **8**, 800 (2012).
- [13] M. Safdar, Q. Wang, M. Mirza, Z. Wang, K. Xu, and J. He, *Nano Lett.* **13**, 5344 (2013).
- [14] S. Safaei, P. Kacman, and R. Buczko, *Phys. Rev. B* **88**, 045305 (2013).
- [15] J. Liu, W. Duan, and L. Fu, *Phys. Rev. B* **88**, 241303 (2013).
- [16] A. Lopez-Otero, *Thin Solid Films* **49**, 3 (1978).
- [17] A. Szczerbakow and H. Berger, *J. Crystal Growth* **139**, 172 (1994).
- [18] G. Springholz and G. Bauer, *Phys. Status Solidi B* **244**, 2752 (2007).
- [19] B. N. Jensen, S. M. Butorin, T. Kaurila, R. Nyholm, and L. I. Johansson, *Nucl. Instrum. Methods Phys. Res. A* **394**, 243 (1997).
- [20] A. Svane, N. E. Christensen, M. Cardona, A. N. Chantis, M. van Schilfgaarde, and T. Kotani, *Phys. Rev. B* **81**, 245120 (2010).
- [21] A. A. Taskin, S. Sasaki, K. Segawa, and Y. Ando, [arXiv:1305.2470v1](https://arxiv.org/abs/1305.2470v1).
- [22] R. A. Bartynski, E. Jensen, T. Gustafsson, and E. W. Plummer, *Phys. Rev. B* **32**, 1921 (1985).
- [23] Ph. Hofmann, Ch. Søndergaard, S. Agergaard, S. V. Hoffmann, J. E. Gayone, G. Zampieri, S. Lizzit, and A. Baraldi, *Phys. Rev. B* **66**, 245422 (2002).
- [24] J. A. Miwa, Ph. Hofmann, M. Y. Simmons, and J. W. Wells, *Phys. Rev. Lett.* **110**, 136801 (2013).
- [25] S. G. Louie, P. Thiry, R. Pinchaux, Y. Petroff, D. Chandresis, and J. Lecante, *Phys. Rev. Lett.* **44**, 549 (1980).
- [26] W. A. Harrison, *Electronic Structure and the Properties of Solids - The Physics of the Chemical Bond* (Freeman, San Francisco, 1980).
- [27] H. Preier, *Appl. Phys.* **20**, 189 (1979).
- [28] J. Liu, T. H. Hsieh, P. Wei, W. Duan, J. Moodera, and L. Fu, *Nat. Mater.* **13**, 178 (2014).
- [29] P. Barone, D. Di Sante, and S. Picozzi, *Phys. Status Solidi RRL* **7**, 1102 (2013).
- [30] Y. Tanaka, T. Shoman, K. Nakayama, S. Souma, T. Sato, T. Takahashi, M. Novak, K. Segawa, and Y. Ando, *Phys. Rev. B* **88**, 235126 (2013).